Monthly Notices of the ROYAL ASTRONOMICAL SOCIETY

MNRAS **435,** 809–821 (2013)
Advance Access publication 2013 August 14

doi:10.1093/mnras/stt1351

Mergers of multimetallic globular clusters: the role of dynamics

Pau Amaro-Seoane,[1★] Symeon Konstantinidis,[2,3] Patrick Brem[1] and Márcio Catelan[2]

[1]*Max Planck Institut für Gravitationsphysik (Albert-Einstein-Institut), D-14476 Potsdam, Germany*
[2]*Departamento de Astronomía y Astrofísica, Facultad de Física, Pontificia Universidad Católica de Chile, Av. Vicuña Mackenna 4860, 782-0436 Macul, Santiago, Chile*
[3]*Astronomisches Rechen-Institut, Zentrum für Astronomie der Universität Heidelberg, Mönchhofstraße 12-14, D-69120 Heidelberg, Germany*

Accepted 2013 July 19. Received 2013 July 19; in original form 2012 March 13

ABSTRACT

Hubble Space Telescope observations of globular clusters (GCs) in the Antennae galaxy show clusters of clusters, or regions in the galaxy that span hundreds of parsec, where many of the GCs are doomed to collide, and eventually merge. Several such objects appear likely to present a significant range in ages, hence possibly metallicities, and their merger could plausibly lead to multimetallic GCs. Here we explore this process with direct-summation *N*-body simulations with graphics processing unit hardware. Our results reveal that colliding GCs with different metallicities and ages can produce a GC with multiplicity and occupation fractions not unlike those observed in multimetallic clusters. In our simulations, the merged clusters have a phase with a larger amount of flattening than average, as a consequence of rapid rotation – thus suggesting that relatively recent mergers may play a role in producing highly flattened, multimetallic clusters. We additionally explore the role of the King parameter of the cluster in the occupation fractions with a set of 160 direct-summation simulations and find that for equal size clusters the King parameter of the progenitor clusters determines the occupation fractions in the merger product, while in unequal size mergers the size of the clusters dominates the distribution of stars in the new GC. In particular, we find that the *observed* distribution of populations in ω Cen can be described to some extent with our dynamical models.

Key words: Hertzsprung–Russell and colour–magnitude diagrams – stars: kinematics and dynamics – globular clusters: general.

1 INTRODUCTION

The merger history of globular clusters (GCs) is increasingly being recognized as an important aspect of GC research (e.g. van den Bergh 1996; Dieball, Grebel & Theis 2000; Dieball, Müller & Grebel 2002; Minniti et al. 2004; Lane et al. 2010; Bekki & Yong 2012; Peacock, Zepf & Finzell 2013, and references therein). In the case of the Milky Way, a merger history has most recently been suggested for NGC 1851, on the basis of detailed spectroscopic analysis of a large sample of red giants (Carretta et al. 2010a, 2011). Indeed, the existence of a small but non-negligible metallicity spread in this cluster had also been suggested previously by Lee et al. (2009), who first hinted that the cluster's metallicity distribution may actually be bimodal.

As pointed out by Catelan (1997), the presence of bimodal, or even multimodal, metallicity distributions is generally expected, in the case of the GC merger scenario originally envisaged by van den Bergh (1996). On the other hand, the empirical evidence suggests that mergers of clusters of different metallicities may have been few in the Milky Way and its immediate vicinity (Catelan 1997). However, the situation may be more favourable in other environments. In particular, in the Antennae galaxy (NGC 4038/NGC 4039), gravitationally bound clusters appear to exist with a sizeable difference in ages, hence possibly also metallicity. These objects will eventually merge – and, if they survive long enough, will eventually lead to GC-like objects with bimodal, and possibly multimodal distributions (e.g. Kroupa 1998; Peacock et al. 2013). In a more general sense, mergers of star clusters may play an important role in the explanation of the complex abundance patterns that are observed in Galactic GCs, which include not only metallicity spreads in massive systems like ω Centauri (NGC 5139) and M54 (NGC 6715), but also evidence of multiple populations, as indicated by the abundances of chemical species such as O, Na, Mg, Al, and also the observed colour–magnitude diagrams (CMDs; e.g. Carretta et al. 2010b, 2011; Bekki 2011, 2012; Joo & Lee 2013, and references therein). In this paper, we will explicitly tackle only the aforementioned *global* metallicity variations.

The purpose of this paper is accordingly to provide the first numerical simulation of a GC merger involving components of different ages and metallicities. Indeed, while other simulations of GC mergers have been carried out by other authors, including

★ E-mail: pau.amaro-seoane@aei.mpg.de

Makino, Akiyama & Sugimoto (1991), Hurley (2003), Dieball et al. (2000), Theis (2001), Portegies Zwart & Rusli (2007) and de la Fuente Marcos & de la Fuente Marcos (2010), to the best of our knowledge, ours is the first study to explicitly track the metallicity of the individual stars in the course of the merger (see also Amaro-Seoane et al. 2012).

Our paper is structured as follows. In Section 2, we provide more details regarding the properties of potential merger progenitors in the Antennae galaxy, as direct motivation for our numerical experiments. In Section 3, we describe our numerical simulations, along with the region of parameter space explored in our calculations. In Section 4 we present our main results, with particular emphasis on the resulting CMDs and the change in cluster shape as a function of time. In Section 5, we show the impact of the size and King parameter on the merger product. In Sections 6 and 7, we present an analysis of the rotation of the merged clusters and the particular case of ω Cen. Finally, in Section 8 we summarize our results and present some additional discussion.

2 SMASHING CLUSTERS WITH DIFFERENT METALLICITIES: ANSATZ AND NUMERICAL TOOLS

Observations of colliding galaxies such as the Antennae galaxy show bound systems of young, massive clusters. In this system, *Hubble Space Telescope* (*HST*) observations exhibit relatively small regions spanning a few hundreds of parsec embracing hundreds or even thousands of young clusters, i.e. clusters of clusters or 'cluster complexes' (CC from now onwards; see e.g. Kroupa 1998; Whitmore et al. 2010, and references therein). These have been proposed to be the progenitors of ultracompact dwarf galaxies (UCDs) or even massive GCs as a result of the agglomeration of hundreds of their member clusters (Fellhauer & Kroupa 2002, 2005; Brüns et al. 2011; Brüns & Kroupa 2011; Amaro-Seoane et al. 2012; Bekki 2012; Peacock et al. 2013).

There are different reasons why two clusters participating in a collision may have different metal contents. For instance, Fe is produced during supernova (SN) explosions, which create a very fast moving gas that cannot be retained in the cluster because of its shallow potential well (unless the cluster was born at least 10 times more massive than it is today; see Renzini 2008; Valcarce & Catelan 2011, and references therein). In a star-forming region, this gas can mix with gas clouds surrounding the parent cluster and, after slowing and cooling down, create a new, younger cluster – the child cluster – with a characteristic stellar Fe abundance higher than the one characterizing the stars of the parent cluster. The child and parent clusters can then merge with one another, giving birth to another cluster with two well-defined stellar populations: the metal-poor (MP) stars of the parent cluster and the metal-rich (MR) stars of the child cluster.

Indeed, recent detailed observations of some of the Antennae galaxy's CCs (such as the 'knot S' and 'knot B'; Whitmore et al. 2010) typically show a single massive cluster older (habitually by a few tens of Myr) than the rest of the members of the CC located at the centre of a giant molecular cloud. Whitmore et al. (2010) suggest that the characteristic location of the older cluster and its age might be explained in terms of interactions between the older cluster and the gas cloud. The difference in age would be an indicator that the giant stars in the old cluster have released gas because of SN explosions, thus polluting the surrounding gas. Therefore, the stars of the new clusters must have a clear-cut different Fe abundance. These CCs might accordingly be a natural breeding ground for multimetallic GCs, because they have different ab initio metallicities, collide and merge. Indeed, evidence of already merged clusters in the Antennae galaxy has been found by Greissl et al. (2010) who observed the spectrum of a massive star cluster of this galaxy and concluded that the cluster is a superposition of a young and an older one with ages below 3 Myr and between 6 and 18 Myr, respectively (see also Peacock et al. 2013). The observed age difference may plausibly be accompanied by a difference in the metallicity of the two populations.

3 NUMERICAL SIMULATIONS: TOOLS AND GENERAL SET-UP

We run direct-summation *N*-body simulations of clusters with initially different metallicity contents and ages to investigate this and analyse the impact of dynamics on the occupation fractions of the different populations in the CMDs.

We set initially the clusters on a parabolic orbit so that the minimum distance at which they pass by is $d_{\rm min}$ if they are considered to be point particles at their centres of mass, as described in Amaro-Seoane (2006). We use a Kroupa (2001) initial mass function (IMF) for the stars of the clusters with mass limits 0.2 and 100 $M_\odot$. We integrate the evolution with direct-summation *N*-body tools, which integrate all gravitational forces for all particles at every time step, without making any a priori assumptions about the system. The code we have employed, NBODY6-GPU, uses the improved Hermite integration scheme (Aarseth 1999, 2003). This needs computation of not only the accelerations, but also their time derivatives. The programme also includes *KS regularization* and *chain regularization*, so that when particles are tightly bound or their separation becomes too small during a hyperbolic encounter, the system is regularized (Kustaanheimo & Stiefel 1965; Aarseth 2003) to prevent too small individual time steps.

We ran different cases with different initial conditions, as shown in Table 1.[1] The clusters, assumed to be isolated, were modelled initially with a King model of different concentrations *W*0 (King 1966), radii and metallicities and evolved for different times with the stellar evolution package SSE, described in Hurley, Pols & Tout (2000). For the particular case $\mathcal{E}$, we use the outcome of simulation $\mathcal{A}$ and make it merge with another cluster (numbered 3) on a parabolic orbit with a new $d_{\rm min,\,2}$ and $R_{\rm COM,\,2}$, as indicated on the right of Table 1. During the collision we neglect stellar evolution, because in all runs it took approximately a few Myr and the impact of evolving the masses on the global dynamics is negligible. We find in our simulations a significant mass loss after the merger of the clusters that affects the different occupational fraction numbers of the CMDs.

4 RESULTS: DIFFERENT DYNAMICAL AND CHEMICAL CONFIGURATIONS

4.1 CMDs and fractional occupation numbers

To determine when the clusters merge, we locate the density centres of the two clusters and that of the merged system following Casertano & Hut (1985). We follow the simulations after the density centres have coincided for about one half-mass relaxation time $T_{\rm rlx,\,h}$ of the final cluster. This allows us to study the distribution of stars due to the dynamics of the system, which is important to

[1] See also http://members.aei.mpg.de/amaro-seoane/ASKBC

Table 1. Initial conditions for the clusters. From the left to the right we have the simulation ID, the cluster number (Cl#), the *W*0 parameter, the initial radius of the cluster, the metallicity and the initial age of the cluster. On the last right-hand column we show the initial distance between the centre-of-mass of the two clusters that collide, $R_{\rm COM}$ (which corresponds to $|\boldsymbol{x}_1 + \boldsymbol{x}_2|$ of fig. 1 in Amaro-Seoane 2006), and $d_{\rm min}$, both in pc. In all simulations but $\mathcal{E}$ we use an initial total number of stars of 60 000 (30 000 for each cluster). In the case of $\mathcal{E}$ we use the outcome of $\mathcal{A}$, which is a cluster of 52 691 stars, and a radius of 20 pc and make it collide with a third cluster, of $N_\star = 20\,000$ stars for $\mathcal{E}$. In this simulation we add the new distance between COM, $R_{\rm COM,\,2}$ and $d_{\rm min,\,2}$ for the second collision. We note that the MR cluster is initially modelled with a higher value of *W*0 because the observations suggest that the MR population may be more centrally concentrated.

	Parameters					
	Cl#	*W*0	*R* (pc)	*Z*	Age (Myr)	Distances
$\mathcal{A}$	1	9	6	0.002	100	$R_{\rm COM} = 12$
	2	5	3	0.001	50	$d_{\rm min} = 0.5$
$\mathcal{B}$	1	12	5	0.006	50	$R_{\rm COM} = 10.6$
	2	5	3	0.005	100	$d_{\rm min} = 0.5$
$\mathcal{C}$	1	12	5	0.02	50	$R_{\rm COM} = 10.6$
	2	5	3	0.01	100	$d_{\rm min} = 0.5$
$\mathcal{D}$	1	9	6	0.002	100	$R_{\rm COM} = 52.8$
	2	5	3	0.001	10	$d_{\rm min} = 2.0$
$\mathcal{E}$	1	9	–	0.002	100	$1 + 2$ from $\mathcal{A}$
	2	5	–	0.001	50	$R_{\rm COM,\,2} = 49$
	3	5	5	0.009	2.1×10^3	$d_{\rm min,\,2} = 10$

understand the impact of mass loss in the CMD and occupational fractions in different shells of mass around the density centre of the merged system. Naturally, the CMD we obtain from the simulations corresponds to idealized observational conditions. In real observations the measurements are affected by both random and systematic errors and completeness. Photometric errors are not constant with apparent magnitude. In general, more luminous stars have smaller photometric errors. This is described in fig. 5 of Stetson, Catelan & Smith (2005) and also in table 2 of Perina et al. (2009), which show the exponential growth of the photometric errors with apparent magnitude. Also, faint stars are hard to detect, so the CMD suffers from completeness (i.e. only a fraction of the faint stars are actually observed). A description of the completeness in the CMD of real clusters is given in fig. 1 of Brown et al. (2003) and also in fig. 9 and table 7 of Buonanno et al. (1994). For the transformation of our theoretical CMD to the 'real' CMD that one would observe, we introduce an exponential function to guide the photometric errors, which are then selected from a Gaussian random distribution. We also included a function for the completeness of the CMD, assuming completeness 100 per cent for stars with high luminosities and 0 per cent for low-luminosity stars.

In Fig. 1 we show the theoretical and observational CMD of simulation $\mathcal{E}$, assuming that the clusters are at a distance of 5 Mpc. As it is obvious, just a fraction of the upper part of the CMD of such a cluster could be observed with future telescopes, but the signature of the merger of three clusters would still be detectable. We can see that at the level of the turn-off (TO) point the subgiant branch (SGB) splits into three well-defined branches, resembling the CMDs presented by Catelan (1997). While such CMDs are not typically found in the Milky Way and its immediate vicinity, they will likely be more commonplace in the Antennae galaxy's GC system, several Gyr from now. This, in turn, suggests that other galaxies with more violent past histories than the Milky Way may also be more likely to harbour such GC systems. Candidate hosts for such multimetallic merged clusters, in this sense, may include M82 (e.g. Keto, Ho & Lo 2005; Wei, Keto & Ho 2012), at a distance of 3.4 ± 0.1 Mpc (Dalcanton et al. 2009), and even M31 itself (e.g. Brown 2006, 2009; Hammer et al. 2010, and references therein), at a distance of 752 ± 27 kpc (Riess, Fliri & Valls-Gabaud 2012).

We then calculate the occupation ratio of the different stellar populations, N_1/N_2 (and $N_3/[N_1 + N_2]$, if we had three different populations) for different shells starting at the density centre. The results are shown in Table 2. The distribution of the different populations in the final, merged cluster depends mostly on the initial size, concentration, metallicities and also on the initial number of stars in each cluster, as well as their IMFs and ages. In most of our models (all but $\mathcal{B}$ and $\mathcal{C}$), the MR cluster, which is always cluster 1, appears to contribute fewer stars to the centre of the merged

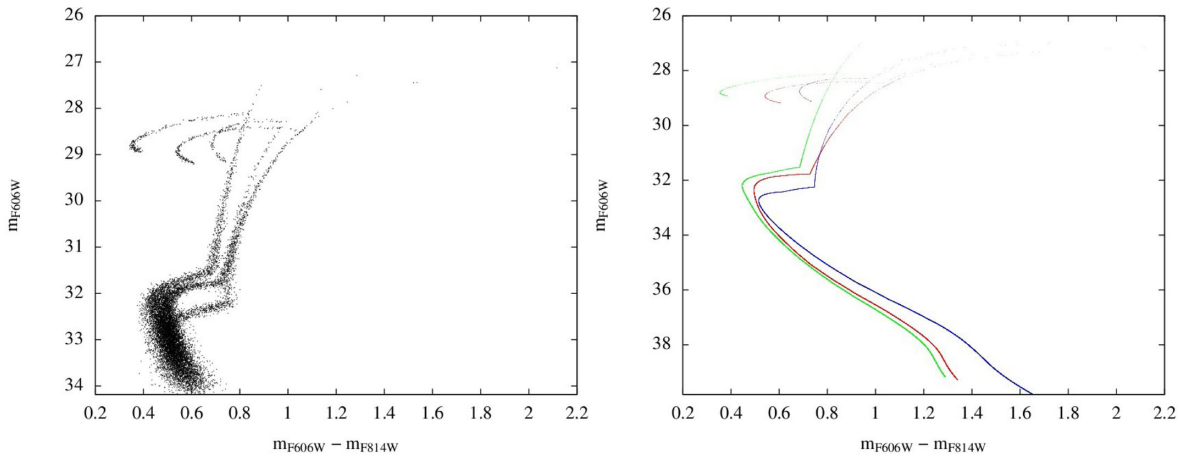

Figure 1. CMD of case $\mathcal{E}$, a collision of a cluster with another cluster which is itself the result of a merger of two clusters (case $\mathcal{A}$), with artificial errors (left-hand panel) and without them (right-hand panel). The first MS (curve with the TO point at ∼0.45 mag in $m_{F606W} - m_{F814W}$ in the right-hand panel, green line in the on-line version of the paper) corresponds to the stellar population of $Z = 0.002$, the next MS to $Z = 0.001$ (red curve of right-hand panel) and the third one to $Z = 0.009$ (blue curve). The clusters that harboured the two first metallicities had an age of 100 and 50 Myr, respectively, and the third one had an age of 10^3 Myr. The CMD is for stars in the shell $0 \leq r/{\rm pc} < 2.5$ after evolving the merged cluster for 10 Gyr. We set the distance of 5 Mpc to convert to apparent magnitudes. The left-hand panel shows the observable CMD of the same cluster.

Table 2. Occupation fraction and maximum ellipticity for the mass fraction 0.5, $\epsilon_{0.5,\,\max}$ (see caption of Fig. 2), for the cases of Table 1. The fractions are given in terms of numbers of stars belonging initially to the first cluster (N_1) and the second one (N_2) for different shells of the resulting merged cluster starting from the density centre. For the last two cases we also give the fraction relative to the third one, N_3.

	N_1/N_2 (and $N_3/(N_1+N_2)$)				
Shell (pc)	Case $\mathcal{A}$	Case $\mathcal{B}$	Case $\mathcal{C}$	Case $\mathcal{D}$	Case $\mathcal{E}$
$0 \le r < 0.5$	0.94	1.25	1.08	0.50	0.85 (0.32)
$0.5 \le r < 1$	0.86	1.02	1.03	0.53	0.80 (0.26)
$1 \le r < 2$	0.72	0.83	0.87	0.61	0.78 (0.23)
$2 \le r < 3$	0.66	0.81	0.82	0.90	0.74 (0.23)
$3 \le r < 4$	0.82	1.00	0.98	1.07	0.79 (0.24)
$4 \le r < 5$	1.03	1.06	1.00	1.25	0.77 (0.27)
$5 \le r < 10$	1.39	1.19	1.17	1.52	0.95 (0.30)
$10 \le r < 50$	1.96	1.42	1.36	2.28	1.31 (0.45)
$\epsilon_{0.5,\,\max}$	0.178	0.215	0.100	0.174	0.298

cluster than the MP population. This appears to be a natural result of the initial parameters chosen and more specifically of the different initial size of the clusters, as we will see below.

ω Cen is the system for which we have the best observational data about the radial distribution of its multiple populations. Bellini et al. (2009) do a detailed study showing that stars belonging to the blue MS (bMS) appear to be more centrally concentrated than stars of the red MS (rMS), with the fraction $N_{\rm bMS}/N_{\rm rMS} < 1$ outside the core of the system. Since the bMS contains stars with greater metallicity, according to the authors, stars with greater metallicity appear to be more centrally concentrated. As shown in Table 2, one of our models ($\mathcal{B}$) shows a distribution in which the MR stars appear more centrally concentrated relative to the MP stars of the merged cluster. In the same model, MP stars appear to dominate the region 1–3 pc, while MR stars again dominate the external shells of the cluster as a result of the large difference in the initial concentration of the two clusters and in their initial size. We caution the reader, however, that ω Cen may be a much more complex case than described by our models, since its progenitor system must have been much more massive in the past (e.g. Renzini 2008; Valcarce & Catelan 2011, and references therein), and the present-day ω Cen is characterized by a broad, continuum metallicity distribution, which we are not in a position to properly describe with our relatively simple N-body models, which imply sharply peaked (if multimodal) metallicity distributions.

In this context, our models may fare somewhat better in the case of NGC 1851. In this case, Carretta et al. (2010b, 2011) observed evidence of a difference in the distribution of the two populations of red giants. According to them, the MP component seems to be more centrally concentrated than the MR one. This observational evidence, which however remains somewhat controversial (Milone et al. 2009; Carretta et al. 2011), contradicts a scenario for the formation of the second population of stars within the same cluster (e.g. Bekki 2011; Valcarce & Catelan 2011), which foresees that the MR population should be more concentrated around the centre. In this sense, the possibility of a merger origin would appear like an interesting alternative.

4.2 Ellipticity

In study of the parameter space, we have found that the result of a collision is a cluster that will exhibit phases in the evolution with ϵ above average. In the particular case of simulation $\mathcal{D}$, the GC

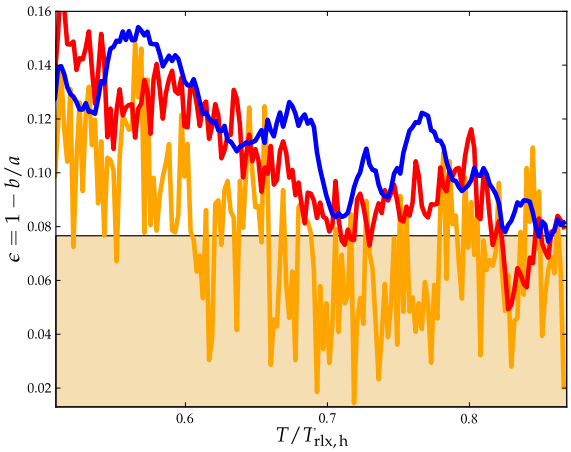

Figure 2. Evolution of ϵ for case $\mathcal{D}$ after the density centres coincide. The semimajor axes are calculated with the ellipsoids of inertia (see e.g. Chandrasekhar 1969) and determined by different mass fractions of the stars (at the lowest value of $T/T_{\rm rlx,\,h}$ in the figure, from the bottom to the top 0.2, 0.5 and 0.8, displayed in orange, red and blue, respectively in the on-line paper). The solid black line shows $\hat{\epsilon}$; thus, values within the coloured box are average. The stars are distributed according to the amount of gravitational energy; hence, the lower the mass fraction is, the closer we are to the centre of the resulted merged system.

achieves average values after almost one $T_{\rm rlx,\,h}$, so that any oblateness would not be present today in clusters older than their half-mass relaxation time, unless the collision happened recently (though we note that we cannot model realistic GCs with our number of stars). This means that GCs, in particular young ones, with ϵ above average, are more likely to harbour populations of stars displaying multimetallicity; i.e. any amount of rotation in GCs with multiple metallicities could be a fingerprint for a dynamical origin.

After the collision, and for a significant fraction of the relaxation time, the resulting cluster has a significant amount of rotation. This depends on the initial conditions such as the impact parameter, the King (1966) parameter $W0$ and the relative velocity.

In Fig. 2 we show ϵ versus time for $\mathcal{D}$. We start the analysis after the three density centres coincide. The system has an ϵ above average during a relatively long time and only after $T \sim 0.9\,T_{\rm rlx,\,h}$ ϵ does it reach the average ~0.08. This suggests that cluster mergers may lead, at least for almost one $T_{\rm rlx,\,h}$, to peculiarly flattened systems, whose flattening may be ascribed to their acquired angular momentum during the merger event. Consequently, a correlation between multimetallic stellar populations, ellipticity and rotation may be expected, in the case of a merger origin. Note that increased ellipticity was also found in the merger simulations presented by de Oliveira, Bica & Dottori (2000) and Theis (2001), among others.

Do multimetallic GCs show systematically high ellipticities and rapid rotation? Unfortunately, a conclusive answer to this question cannot be provided at present, given the exceedingly small number of known multimetallic GCs in the local Universe. Still, some of the available evidence appears quite suggestive. ω Cen, in particular, is well known to be one of the most oblate Galactic GCs, as also confirmed by the recent, homogeneous measurements of 116 GCs presented by Chen & Chen (2010), based on Two Micron All-Sky Survey (2MASS) images. ω Cen has rotational velocity $v_{\rm rot}/\sigma = 0.32$–$0.41$, which makes it one of the fastest rotating GCs in the Galaxy. This could be a signature for an agglomeration process of a cluster in a CC which receives more and more impacts from other lighter clusters and 'runs away' in mass, on its way to

forming a UCD. Measurements of the rotation of the 650 stars of ω Cen (Pancino et al. 2007) show that all subpopulations rotate as a single one (see also Anderson & van der Marel 2010, for a study of the proper motions of the subpopulations that supports this result). This can also be explained in terms of a collision between GCs, which would assign all stars the same amount of rotation regardless of their population.

Other Galactic GCs for which a metallicity spread has recently been claimed include M22 = NGC 6656 (e.g. Marino et al. 2011; Alves-Brito et al. 2012) and NGC 2419 (Cohen et al. 2010), both of which are also significantly flattened (Chen & Chen 2010). In fact, Brüns & Kroupa (2011) have suggested that the latter cluster may be the result of a merged star cluster complex, during the interaction between a gas-rich galaxy and the Milky Way. Very recently, Bekki (2012) has also considered the possibility that such clusters may originate from mergers, with the possible production of multimodal metallicity distributions.

Interestingly, Gennaro et al. (2011) have suggested that the observed elongation of the starburst cluster Westerlund 1 may similarly be ascribed to mergers. On the other hand, one should be careful to note that GC ellipticities may be due to a variety of physical mechanisms, which are not always easy to disentangle. For instance, Stephens, Catelan & Contreras (2006) note that the GC WLM-1 in the Wolf–Lundmark–Melotte (WLM) dwarf galaxy in the Local Group, in spite of being one of the most elongated GCs known, and of being subject to very minor tidal stresses, does not show any evidence of rotation. We are clearly in face of a very complex phenomenon, which cannot be explained in terms of any simple scenario. Still, it does appear like mergers may play an important role in at least some cases, and we accordingly suggest that the connection between multimodal metallicity distributions, ellipticity and rotation be further explored, whenever GC candidates with multiple metallicities may be detected.

5 A DETAILED STUDY OF THE FRACTIONAL OCCUPATION NUMBER AS A FUNCTION OF THE KING PARAMETER, BASED ON CASE $\mathcal{A}$

5.1 Initial data set-up

In order to understand the impact of the King parameter $W0$ in the final distribution of different populations as a function of the distance from the density centre of the merged system, we run a set of 128 simulations with a set-up that has the same initial numerical set-up as case $\mathcal{A}$ of Table 1 and the same ages. We explore different parameters, and only fix the number of stars, the radii and metallicities, as summarized in Table 3. In this first exploration we set cluster 2 to have half the size of cluster 1.

We hence vary in the initial data the $W0$ King parameter (i.e. $W0_1$ for cluster 1 and $W0_2$ for cluster 2) and choose the values of 3, 6, 9 and 12. This gives us 16 possible combinations for the two parameters. For each combination we run eight different realizations with initial random seeds to improve the statistics. Therefore, the whole set comprehends 128 models.

Table 3. Fixed parameters for the detailed analysis of case $\mathcal{A}$ of the role of the King parameter. The total mass of the system is 60 000 $M_\odot$.

Cluster	N	R (pc)	Z	Age (Myr)
1	30 001	6	0.01	50
2	30 001	3	0.04	100

Initially we set up the clusters as explained in Section 3 and we choose a Kroupa IMF with lower mass 0.2 $M_\odot$ and higher mass 50 $M_\odot$ (Kroupa 2001).

To evolve the clusters to the assumed initial age, as in the previous section, we use SSE, which uses the metallicity Z and age of each cluster. Hence, our complete set-up for one simulation is two clusters in a parabolic orbit with their stars evolved to the specified initial age.

We can see in Fig. 3 the mass function of the two clusters at $t = 0$ and after 50 and 100 Myr of stellar evolution, as well as the corresponding slopes.

The lower panels of Fig. 3 show the mass function of the two clusters after evolving their stars to their initial age. As expected, because of the small time-scale for stellar evolution (50 and 100 Myr for clusters 1 and 2, respectively), only massive stars have changed significantly their mass with some of them evolving to black holes with lower mass than their progenitors.

We run the dynamical evolution of the clusters for at least one half-mass relaxation time of the final cluster in all simulations, typically to $\sim 1.5\, T_{\rm rlx,h}$.

In Table 4 we present the results for the whole set of simulations. We can see that the dependence on the choice for the King parameter is very weak. What dominates the evolution in this case is the difference of sizes. This is why we average over all King parameters in the table.

We notice that the fraction N_1/N_2 is smaller than 1 until $r \sim 4$ pc in all simulations. Below $r = 3$ pc, N_1/N_2 is smaller than 0.5, meaning that below this radius the number of stars of cluster 2 is more than twice those of cluster 1. In the shell $3 < r \leq 5$ the two clusters have almost equal number of stars. Finally, in the outer shells of the final merged cluster, it is stars originally from cluster 1 which dominate. For $10 < r \leq 50$ cluster 1 has more than three times the stars of cluster 1. Since we have chosen cluster 1 with twice the size of cluster 2, the centre of the systems after merger is more populated with stars that originally belonged to cluster 2, which was more compact. Accordingly, in the outskirts of the merged cluster we find that stars from cluster 1 dominate the population. In our idealized modelling the systems are isolated but if we added an external galactic potential, tidal forces would remove more stars of cluster 1 from the system.

Since the difference in initial sizes plays an important role in the distribution of stars, in order to understand the impact of the choice for the initial King parameters we must address the results by first comparing those simulations which had the same $W0$ for the two clusters. We hence filter the results of Table 4 in which $W0_1 = W0_2 = 3, 6, 9, 12$, respectively, in Table 5. In Fig. 4 we present graphically the results of this table. We can conclude from the results that inside a radius $R \sim 3$ pc (which is close to the half-mass radius), higher $W0$ parameters lead to higher N_1/N_2. This is true for all cases except $W0 = 12$, which has a lower fraction than $W0 = 9$, but still higher than $W0 = 6$. On the other hand, for $R > 3$ pc, an initially higher $W0$ parameter leads to a lower fraction N_1/N_2, again with the exception of $W0 = 12$. The reason for this is that King models of $W0 > 9$ have a very dilute core with very few stars in it. In Fig. 5 we depict the core mass normalized to the total mass and the enclosed mass as a function of the radius and King parameter.

After this first analysis, we now address the results for which the initial King parameters are different. We depict in a three-dimensional figure the final distribution of fractional occupation numbers as a function of the radius and the King parameters in Figs 6 and 7. In the first one we keep $W0_1$ constant (set to 3, 6,

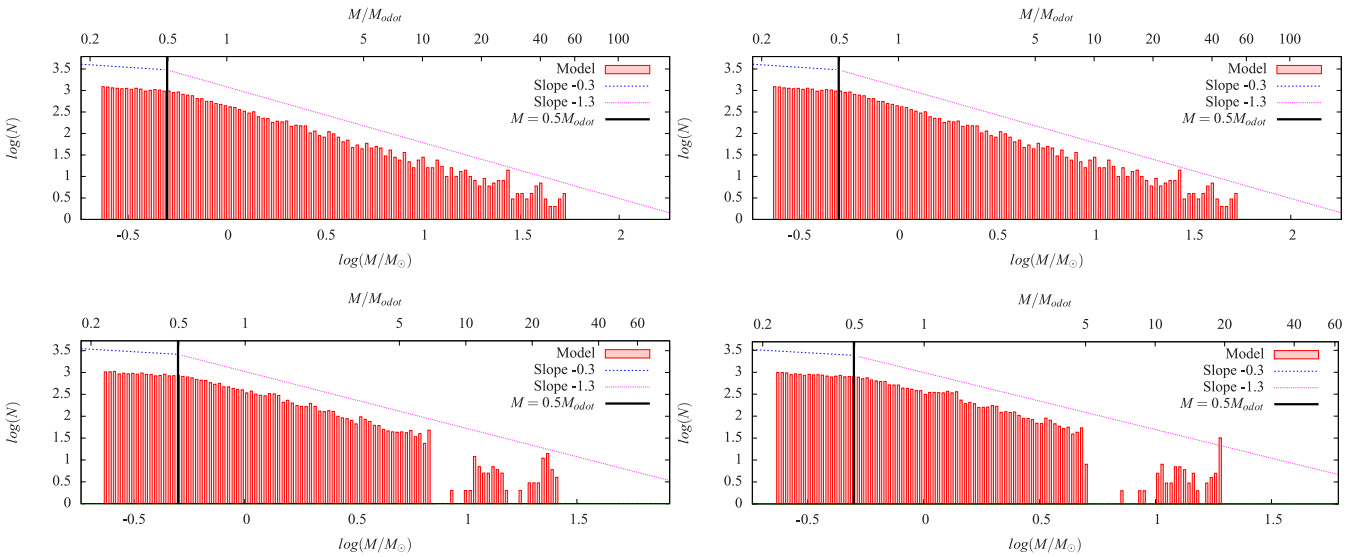

Figure 3. Upper panels: IMF of cluster 1 (left) and cluster 2 (right) at $t = 0$. The slopes of the Kroupa IMF are also shown. The transition from one slope to another happens at 0.5 $M_{\odot}$. Lower panels: same at $t = 50$ Myr ($Z = 0.01$) and $t = 100$ Myr ($Z = 0.04$) for clusters 1 and 2, respectively.

Table 4. Fractional population number for the initial set of simulations in which one of the clusters has a radius twice as large as the other one, for all King parameters.

Shell (pc)	N_1/N_2			
$0 < r \leq 0.5$	0.384 ± 0.083	0.395 ± 0.073		
$0.5 < r \leq 1$	0.399 ± 0.071			
$1 < r \leq 2$	0.514 ± 0.081	0.609 ± 0.091	0.534 ± 0.074	
$2 < r \leq 3$	0.804 ± 0.128			0.639 ± 0.072
$3 < r \leq 4$	1.150 ± 0.148	1.259 ± 0.138		
$4 < r \leq 5$	1.456 ± 0.156			
$5 < r \leq 10$	2.029 ± 0.349			
$10 < r \leq 50$	3.432 ± 1.164			

Table 5. Occupation fractional number for the models of Table 4 in which initially $W0_1 = W0_2$. A graphical representation of these results is in Fig. 4.

Shell (pc)	N_1/N_2			
	$W0_1 = W0_2 = 3$	$W0_1 = W0_2 = 6$	$W0_1 = W0_2 = 9$	$W0_1 = W0_2 = 12$
$0 < r \leq 0.5$	0.276 ± 0.007	0.319 ± 0.016	0.557 ± 0.002	0.443 ± 0.011
$0.5 < r \leq 1$	0.297 ± 0.004	0.342 ± 0.009	0.536 ± 0.006	0.447 ± 0.014
$1 < r \leq 2$	0.457 ± 0.018	0.482 ± 0.007	0.563 ± 0.019	0.499 ± 0.008
$2 < r \leq 3$	0.842 ± 0.025	0.834 ± 0.021	0.710 ± 0.014	0.712 ± 0.018
$3 < r \leq 4$	1.325 ± 0.039	1.185 ± 0.024	0.923 ± 0.029	1.039 ± 0.040
$4 < r \leq 5$	1.765 ± 0.085	1.532 ± 0.052	1.168 ± 0.035	1.353 ± 0.067
$5 < r \leq 10$	2.592 ± 0.080	2.177 ± 0.021	1.702 ± 0.070	1.914 ± 0.042
$10 < r \leq 50$	5.145 ± 0.215	3.833 ± 0.075	2.605 ± 0.083	3.149 ± 0.119

9 and 12) and we vary $W0_2$, and vice-versa in the second figure. We can see that the King parameter only leaves a fingerprint for the outer shells of the merged system in the first figure, and even more remarkably on the second one, which also shows a more clear domination on the number fraction of stars which initially belonged to cluster 1. The two figures are not symmetric in the distribution of N_1/N_2 along the radius because of the initial difference in size, which is the dominant effect here. Since cluster 2 had initially half the size of cluster 1 in all cases, only for low values of $W0$ of cluster 2 we can see a clear domination of N_1 over N_2.

5.2 Equal-size clusters

From the previous analysis we have seen that the size of the clusters very likely plays a dominant role in the distribution of the different populations as a function of the radius of the merged system. To shed light on this dependence, we present in this section a second set of simulations which are identical to the previous set presented before but for the radii of the two clusters, which we fix to 3 pc in the two clusters. We follow the structure of the first set of simulations and use different $W0$ parameters ($W0_1$ and $W0_2$): 3, 6, 9 and 12

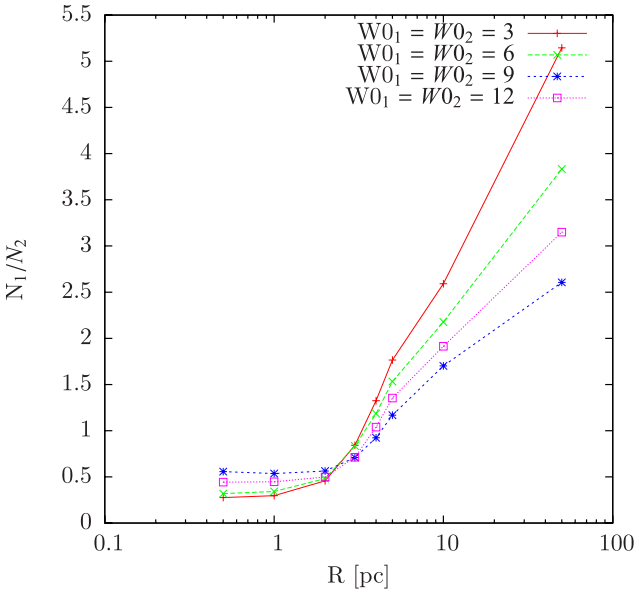

Figure 4. Fraction N_1/N_2 in different shells inside the final cluster at $T = 1000$, for the cases where the two clusters have equal W0 King parameters and different sizes.

for the two clusters. This gives 16 possible combinations and this time we perform two realizations per combination, which makes in total 32 simulations. We set all other set-up parameters (IMF, orbital parameters, age) identical to the first set, so as to be able to understand the role of the size and King parameter more clearly.

We run all simulations for $T = 1200$ N-body units, which corresponds to at least one half-mass relaxation time in all cases. In most of the simulations, the two clusters merge before $T = 50$ time units, in the sense that they share the same density centre, but the occupation fractions will still change significantly after this time. We hence integrate the merged system further until we reach at least ∼20 times the merger time.

We first present the results for the simulations where the two clusters have the same $W0$ parameters. The results are summarized in Table 6 and Fig. 8. We can see that in all cases $N_1/N_2 > 1$ at

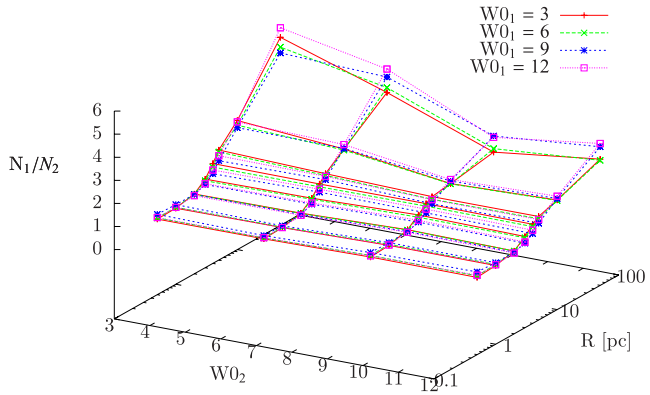

Figure 6. Fraction N_1/N_2 in different shells inside the final cluster at about $\sim 1.5\,T_{\rm rlx,h}$, for the cases in which $W0_1$ is fixed to 3, 6, 9 and 12, while $W0_2$ is free. In these simulations cluster 1 had twice the size of cluster 2.

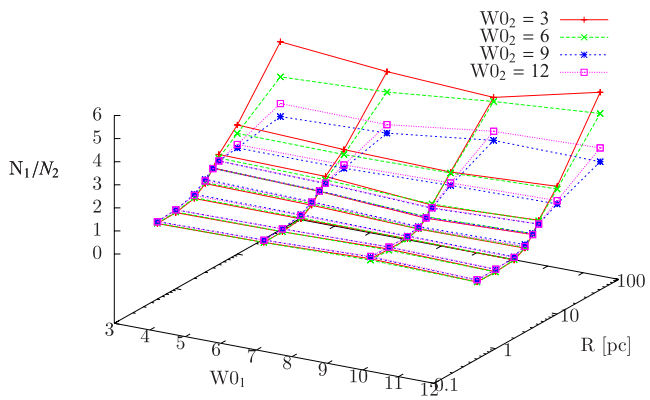

Figure 7. Similar to Fig. 6 but for the cases in which $W0_2$ takes values 3 and 6, while $W0_1$ takes all values.

the centre, and the ratio progressively decreases in the outer shells. This reveals the influence of the different metallicity and age of the two clusters. Cluster 1 is younger and has a lower metallicity (50 Myr old, $Z = 0.01$), and thus it contains a larger number of

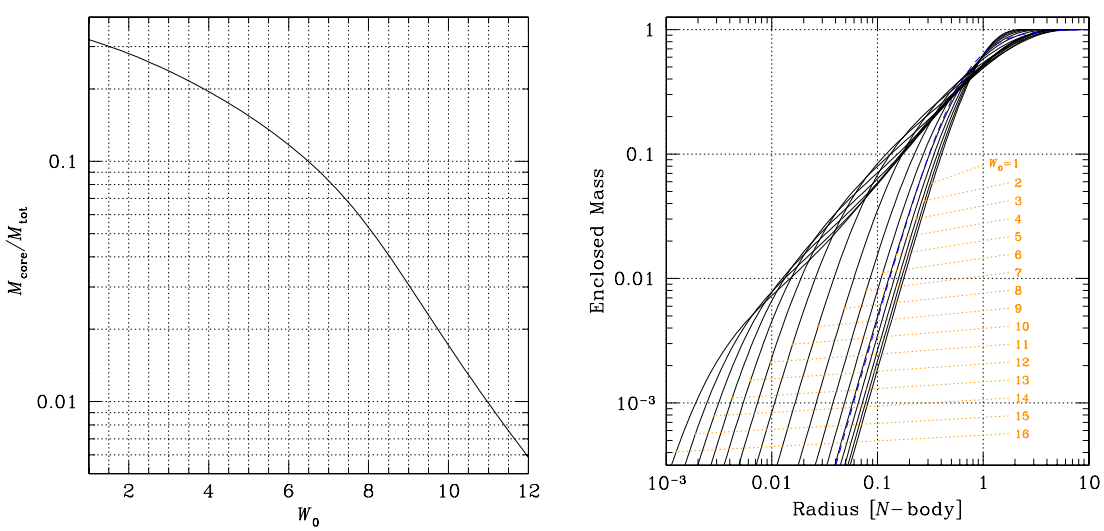

Figure 5. Left-hand panel: core mass in units of the total mass as a function of the King parameter $W0$. The value $W0 = 12$ has a very small core with a tiny fraction of the total mass in it. Right-hand panel: enclosed mass within a certain radius as a function of that radius for different $W0$, ranging between 1 and 16.

Table 6. Summary of the results for simulations with $W0_1 = W0_2$ for clusters that initially have the same size.

Shell (pc)	N_1/N_2			
	$W0_1 = W0_2 = 3$	$W0_1 = W0_2 = 6$	$W0_1 = W0_2 = 9$	$W0_1 = W0_2 = 12$
$0 < r \leq 0.5$	1.150 ± 0.048	1.182 ± 0	1.356 ± 0.014	1.169 ± 0.044
$0.5 < r \leq 1$	1.178 ± 0.027	1.082 ± 0	1.193 ± 0.034	1.144 ± 0.0004
$1 < r \leq 2$	1.096 ± 0.007	1.124 ± 0	1.136 ± 0.008	1.074 ± 0.002
$2 < r \leq 3$	1.002 ± 0.009	1.012 ± 0	1.040 ± 0.015	0.995 ± 0.019
$3 < r \leq 4$	0.939 ± 0.011	0.960 ± 0	0.977 ± 0.013	0.998 ± 0.025
$4 < r \leq 5$	0.927 ± 0.044	0.993 ± 0	0.907 ± 0.005	0.959 ± 0.026
$5 < r \leq 10$	0.917 ± 0.004	0.930 ± 0	0.906 ± 0.020	0.942 ± 0.019
$10 < r \leq 50$	0.847 ± 0.01	0.821 ± 0	0.838 ± 0.024	0.903 ± 0.024

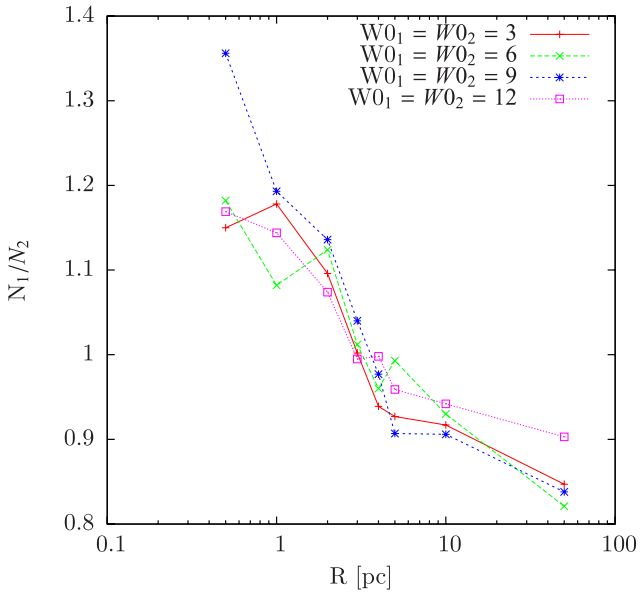

Figure 8. Fraction N_1/N_2 in different shells inside the final cluster at approximately $1.5\,T_{\rm rlx,h}$, for the cases where the two clusters have equal $W0$ King parameters and initial sizes.

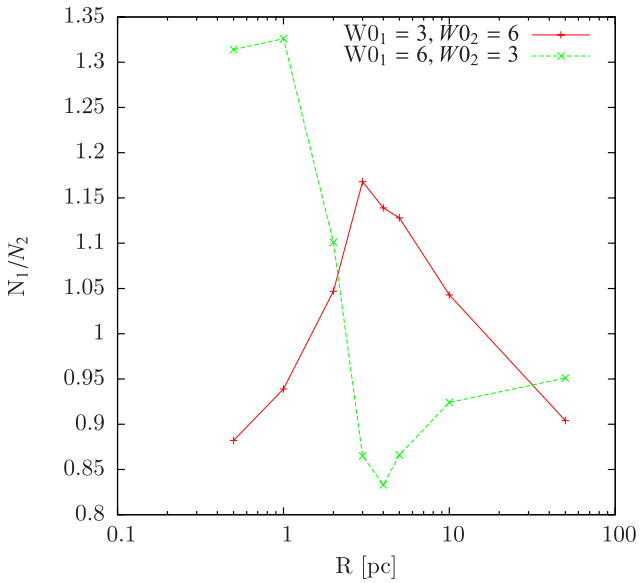

Figure 9. Same as in Fig. 8 for the cases where the two clusters have $W0_1 = 3$, $W0_2 = 6$ and $W0_1 = 6$, $W0_2 = 3$.

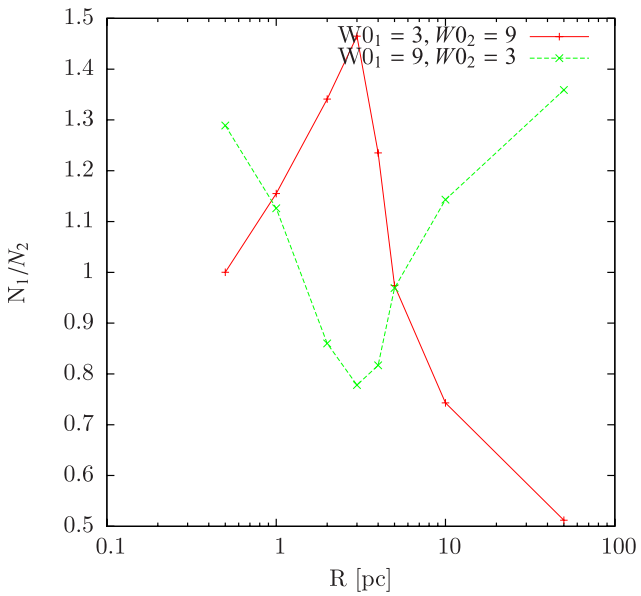

Figure 10. Same as in Fig. 8 for the cases where the two clusters have $W0_1 = 3$, $W0_2 = 9$ and $W0_1 = 9$, $W0_2 = 3$.

massive stars than cluster 2 (100 Myr old, $Z = 0.04$). Massive stars tend to concentrate at the centre of the final cluster, because of mass segregation (see e.g. Khalisi, Amaro-Seoane & Spurzem 2007). Thus, the centre is expected to contain more stars of cluster 1 than cluster 2. Accordingly, lower mass stars populate mainly the outer parts of the system, thus cluster 2 dominates there as it contains more lower mass stars.

We can see this more clearly by reading numbers in Fig. 3. After stellar evolution, cluster 1 has about 400 stars with $m > 5\,\mathrm{M}_\odot$, while cluster 2 has only about 110 stars. Also, cluster 1 has about 1100 stars with $m > 3\,\mathrm{M}_\odot$, while cluster 2 only about 830. Since massive stars tend to concentrate at the centre, cluster 1 dominates there. Finally, cluster 1 has about 23 900 stars with $m < 1\,\mathrm{M}_\odot$, while cluster 2 has about 24 300 stars in the same mass range. Those are low-mass stars that are concentrated outside of the centre of the cluster, thus cluster 2 dominates in the outer parts of the final cluster.

We now address the simulations in which $W0_1 \neq W0_2$. The aim here is to investigate the influence of the King parameter in the final radial distribution of the two populations. In Figs 9–14 we present the results of simulations for which we have taken $W0_1 = X$, $W0_2 = Y$ and $W0_1 = Y$, $W0_2 = X$, with $X \neq Y$. The results in most of the cases

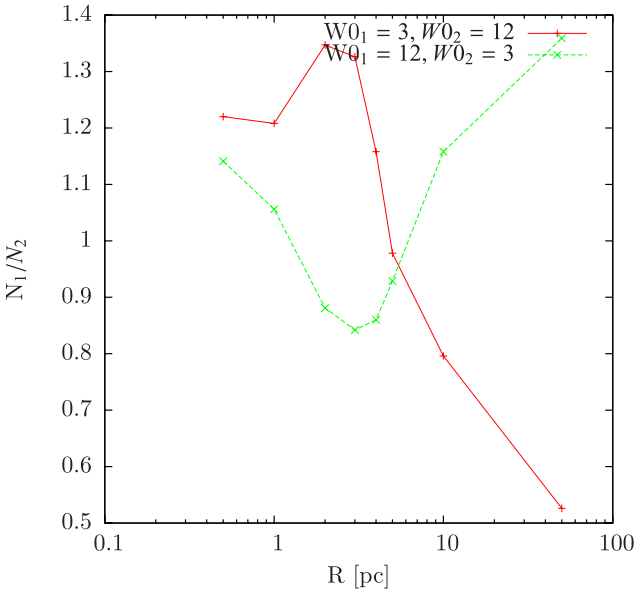

Figure 11. Same as in Fig. 8 for $W0_1 = 3$, $W0_2 = 12$ and $W0_1 = 12$, $W0_2 = 3$.

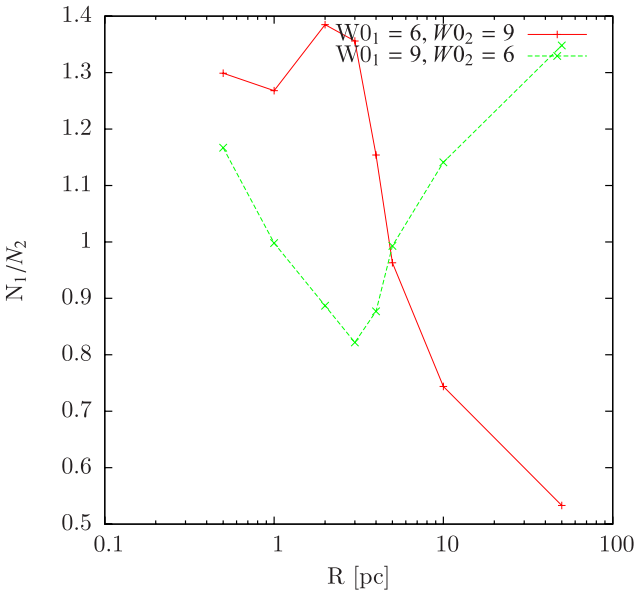

Figure 12. Same as in Fig. 8 but for $W0_1 = 6$, $W0_2 = 9$ and $W0_1 = 9$, $W0_2 = 6$.

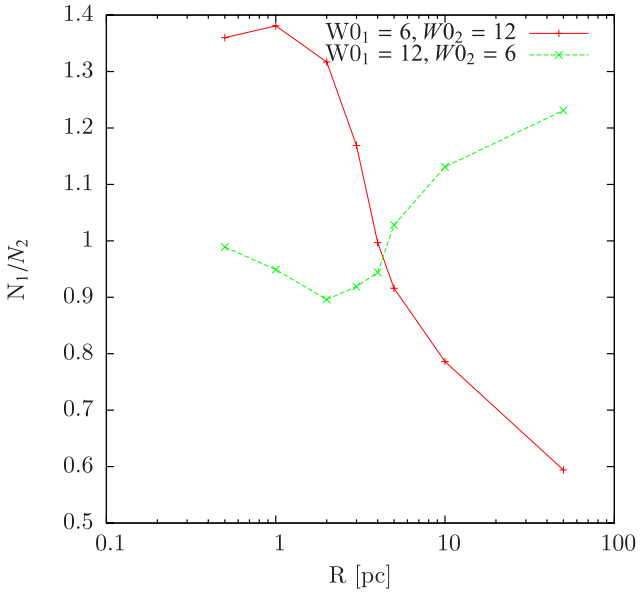

Figure 13. Same as in Fig. 8 for $W0_1 = 6$, $W0_2 = 12$ and $W0_1 = 12$, $W0_2 = 6$.

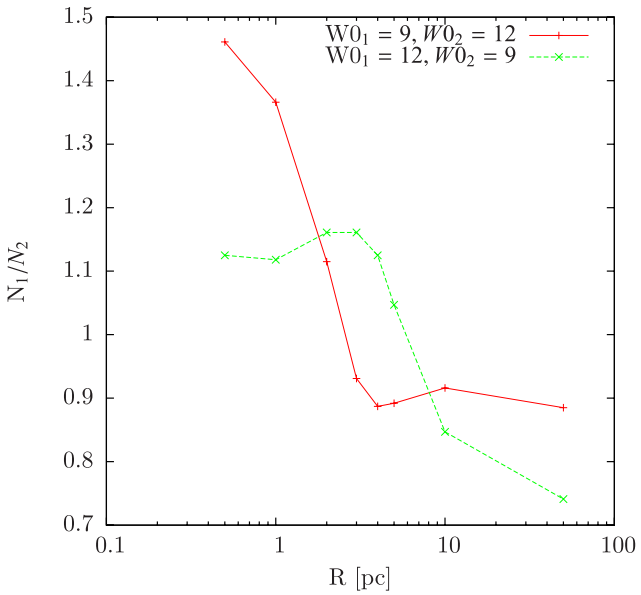

Figure 14. Same as in Fig. 8 for $W0_1 = 9$, $W0_2 = 12$ and $W0_1 = 12$, $W0_2 = 9$.

show that the two lines [line for $W0_1 < W0_2$ (red) and line for $W0_1 > W0_2$ (green)] are almost mirror copies of each other.

In all cases except where $X = 9$ and $Y = 12$, the $W0_1 < W0_2$ line shows its maximum at about the same distance from the centre at which the $W0_1 > W0_2$ shows its minimum. The distance where the lines show their peaks ranges from 1 to 3 pc, which is close to the half-mass radius of the cluster. The biggest difference between the two peaks is found in the case $X = 3$, $Y = 9$. In the exceptional case with $X = 9$ and $Y = 12$, as we discussed before, the two lines are again almost mirror copies of each other, but this time, contrary to all other cases, the very dilute core results in a $W0_1 < W0_2$ line that shows a minimum while the $W0_1 > W0_2$ is a maximum.

In all cases except those in which $X = 3$, $Y = 9$ and $X = 9$, $Y = 12$, the outer parts of the cluster are dominated by cluster 2, for $W0_1 < W0_2$ (the red lines have $N_1/N_2 < 1$ in the outer shells), while cluster 1 dominates the outer parts for $W0_1 > W0_2$ (the green lines have $N_1/N_2 > 1$ in the outer shells). In the inner parts of the cluster the situation is more complicated, since the influence of the King parameters is mixed with the influence of the stellar evolution and the fact that the massive stars of cluster 1 are more numerous than those of cluster 2.

6 A STUDY OF THE ROTATION

In this section we present a brief analysis of the rotation of the merged clusters for the case in which they initially had the same size. We study the rotation as a function of the radius by calculating

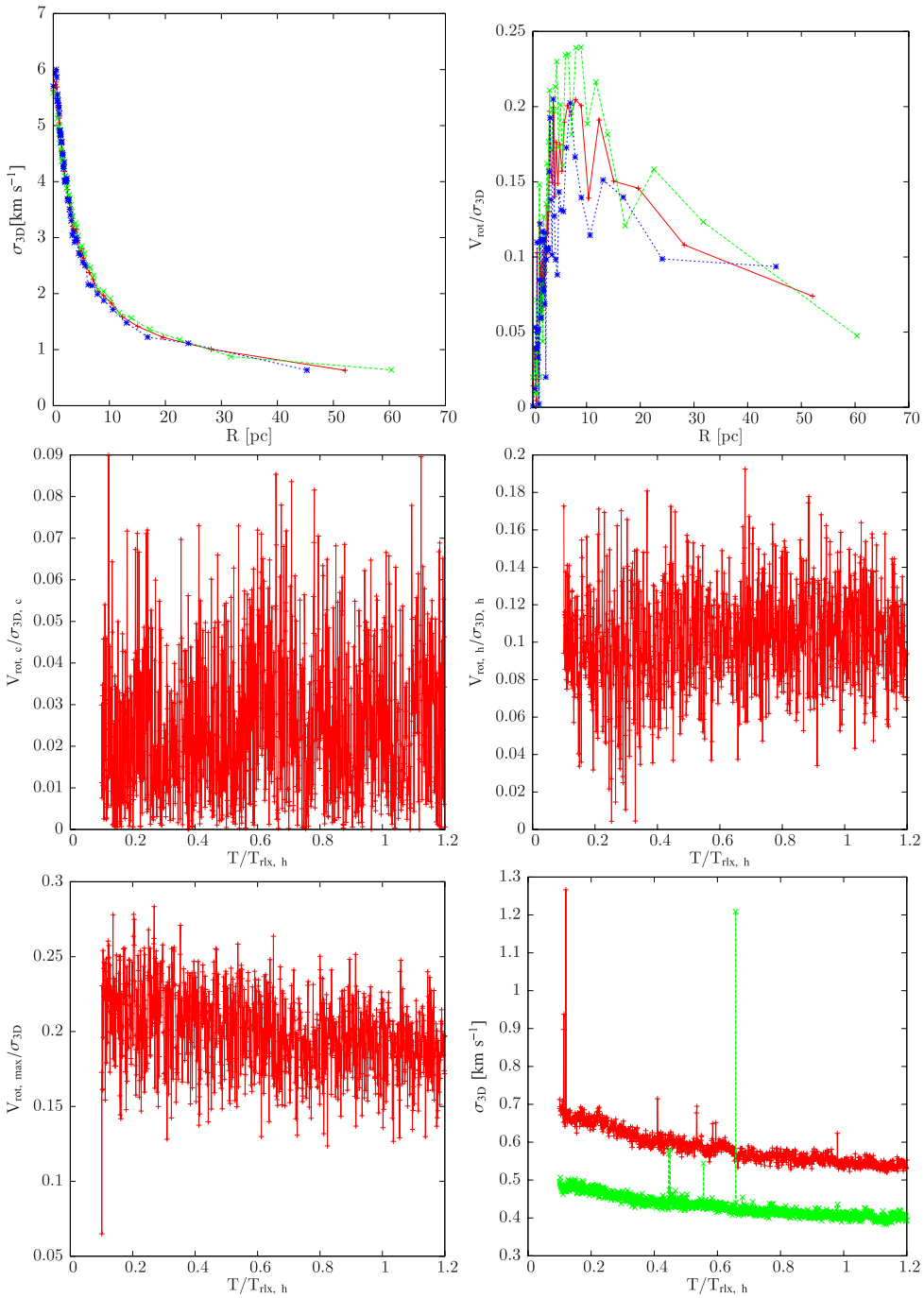

Figure 15. From the left to the right and from the top to the bottom and for the simulation in which the clusters had initially the same size and King parameters 9 and 6, we depict the following quantities. The 3D velocity dispersion σ_{3D} of the merged cluster as a function of the radius R at the end of the simulation, which happens at $1.2\,T_{rlx}$, the rotational velocity V_{rot} of the merged cluster normalized to σ_{3D} as a function of R. The evolution of V_{rot} at the core radius, $V_{rot,c}$ normalized to the core 3D velocity dispersion $\sigma_{3D,c}$, the evolution of the half-mass rotational velocity $V_{rot,h}$ normalized to the half-mass 3D velocity dispersion $\sigma_{3D,h}$, the evolution of the maximum rotational velocity $V_{rot,max}$ normalized to σ_{3D} and the evolution of σ_{3D}. The solid, red lines correspond to the total merged cluster, while we show stars which originally belonged to cluster 1 in dashed, blue lines with star symbols and in dashed, greed lines with crosses to cluster 2.

different quantities. In Fig. 15 we show a set of plots for a representative case, in particular the second iteration of the simulation in which initially $W0_1 = 9$ and $W0_2 = 6$. The fact that the clusters have merged is reflected in the first panel, since the three 3D velocities dispersions are distributed very similarly over the radius of the final cluster. The maximum value is reached at about ∼10 pc from the density centre, resulting in a significant rotation even after $1.2\,T_{rlx}$. The next two panels show the rotational velocity evolution normalized to the velocity dispersion at two relevant radii, the core radius and the half-mass radius. The second panel of the middle row shows us that, although with fluctuations, the high values reached at the inner parts of the cluster are kept during the evolution

Table 7. $V_{\rm rot}/\sigma$ at different radii for the different King parameters considered, in the case of same sizes. In each cell we display the value at the core radius, $R_{\rm c}$, the half-mass radius, $R_{\rm h}$, and the radius in which the merged cluster delivers the maximum value of $V_{\rm rot}$, $R_{V_{\rm max}}$, from the top to the bottom, respectively, along with the deviation that we obtained from the corresponding number of simulations for every combination of King parameters.

$V_{\rm rot}/\sigma$		$W0_1$			
		3	6	9	12
		0.090 ± 0.011	0.042 ± 0.012	0.037 ± 0.029	0.043 ± 0.013
	3	0.149 ± 0.036	0.136 ± 0.016	0.120 ± 0.023	0.117 ± 0.005
		0.186 ± 0.017	0.178 ± 0.026	0.164 ± 0.038	0.153 ± 0.001
		–	0.046 ± 0.003	0.009 ± 0.004	0.026 ± 0.001
	6	–	0.138 ± 0.024	0.060 ± 0.012	0.154 ± 0.040
		–	0.224 ± 0.003	0.151 ± 0.020	0.195 ± 0.001
$W0_2$		–	–	0.012 ± 0.008	0.039 ± 0.005
	9	–	–	0.100 ± 0.005	0.108 ± 0.028
		–	–	0.227 ± 0.007	0.189 ± 0.019
		–	–	–	0.029 ± 0.008
	12	–	–	–	0.062 ± 0.003
		–	–	–	0.182 ± 0.061

of the simulations, to achieve values between 0.07 and 0.12 after 1.2 $T_{\rm rlx}$. The rotational velocities for all other simulations are shown in Table 7. Although it would be important to study the evolution of rotation over longer time spans, we cannot afford it with our code. The last two panels show the maximum rotational velocity as a function of time, which shows a clear slow decay towards lower values and the evolution of the 3D velocity dispersion in the cluster.

7 THE PARTICULAR CASE OF ω CEN

In our simulations we are limited in our study of the vast parameter space by our code. While direct-summation techniques are very robust, they scale typically as $\propto N^2$. Moreover, the approach we use to evolve the clusters and their metallicities is rather simplistic compared to what happens in real clusters. Nevertheless, in Fig. 16 we present a comparison of our scenario with observations of ω Cen, in particular with the data presented in the work of Bellini et al. (2009). In the left-hand panel of the figure we can see that the observed data of ω Cen follows the trend of the shape of the rest of curves at smaller radii. While we are not limited in our resolution at smaller radii, observations are but, on the other hand, we are comparing a very massive cluster, actually an UCD with a model of two clusters of 30 000 stars each. At larger radii, the observed data of ω Cen suit best the model in which the two clusters had a King parameter of 6. On the right-hand panel we observe the same discrepancy that we already had in our Figs 4 and 8 at larger radii. Therefore it seems that ω Cen was probably formed out of the merger of clusters that initially had a similar size, mass and King parameter. Nonetheless, the star resolution is well below the number of stars that we expect in ω Cen, and the simulations might depend on the masses and sizes of the simulated clusters, so that this result should be taken carefully but, in any case, is an encouraging motivation for further probing this scenario.

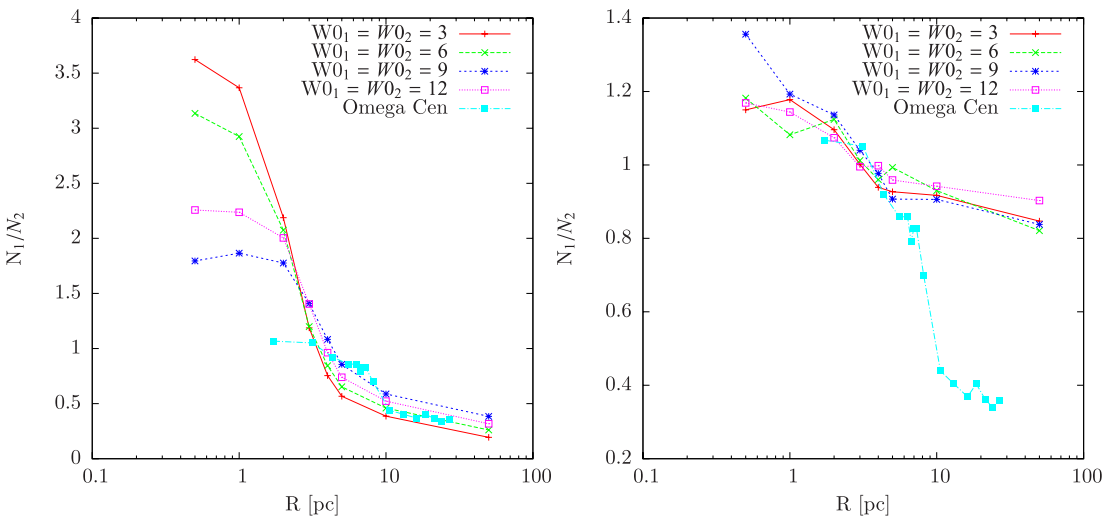

Figure 16. Fractional occupation numbers as a function of the radius as observed in ω Cen (cyan, solid curve with squares), compared to our models for clusters that initially had the same size, left-hand panel, and in the right-hand panel clusters that formed out of the merger of two clusters with different radii, as explained in Section 5.

8 SUMMARY

Motivated by the seemingly unavoidable future merger of clusters with different ages – and hence with potentially different metallicities – in the Antennae galaxy, in this paper we have presented direct-summation *N*-body simulations of such a merger process. Such mergers were addressed in the past by different authors, but ours is the first study to explicitly tackle the possibility of multiple metallicities being present in the merging clusters.

Interacting galaxies such as the Antennae are natural loci for multimetallic clusters to collide. In the Antennae, CCs have been observed with the *HST* and they are the natural birth-place of UCDs, as explained previously. While dynamics does not affect the shape of the resulting CMD of the merged system, it impinges the number of stars in different radial regions of the resulting merger: the occupation fraction will vary with radius, because of the dynamics.

In the first part of this paper we have run a sample of simulations in which we vary all relevant parameters for the final distribution of stars in the merged cluster. We conclude that the initial concentration of the clusters, metallicities, initial ages and sizes play an important role in the final distribution. The differences in the features of the original clusters may well be observed in the CMD of the final cluster, which consists of multiple lines, which might appear merged together in the lower part of the diagram, but could be clearly distinguishable in its upper part, even if the distance to the cluster is up to 5 Mpc. We note that our simulations show that clusters that are created by mergers of smaller clusters exhibit phases with ellipticity above the observational average. This indicates that future observations of young clusters hosting multiple stellar populations should focus on oblate cluster with high rotation.

In the second part of the paper we perform an exhaustive analysis of the role of the King parameter and the size of the clusters in the final distribution of stars. We adapt case $\mathcal{A}$ as our fiducial scenario and fix the number of stars, the metallicity and age.

We start by fixing the size of the clusters, so that one is twice as large as the other one and run 128 simulations (of eight realizations of each combination of $W0$ King parameters to vary the random seed). We find that the dominant parameter on the final distribution of stars is the initial difference of sizes of the clusters. Almost totally independent on the rest of parameters the occupation fractional number is $N_1/N_2 < 1$ closer to the centre of the cluster and >1 outside in all simulations.

We then investigate the role of the metallicity and age by running a set of 32 simulations in which the two clusters have equal sizes. In most of the cases, and independently of $W0$, the core of the final cluster is dominated by stars from cluster 1. However, the outer parts of the systems are mostly affected by the initial difference in the choice for $W0$.

Although we cannot add abundance ratios for many different chemical species to our models, our analysis provides guidance into some possible observational signatures of merger events, including the possible presence of increased rotation and high ellipticity, associated with the existence of multiple metallicities in individual, present-day GCs.

In particular, it is remarkable to see that the set of models in which the clusters had initially the same size leads to a distribution of occupational fractions rather close to what is *observed* in ω Cen. Therefore, in this scenario in which different populations are a fingerprint of cluster mergers, ω Cen was formed out of collisions among clusters with relatively similar sizes, which is reasonable, since ω Cen has been proposed to have formed in a cluster complex dynamically, and the clusters that lead to the formation of a runaway seed UCD have a similar mass and size, due to mass segregation, as in the work of Amaro-Seoane et al. (2012).

ACKNOWLEDGEMENTS

It is a pleasure to thank Marc Freitag, Andrea Bellini and Pavel Kroupa for comments on the manuscript. We are indebted to Jarrod R. Hurley for his assistance with the stellar evolution SSE package, as well as to Peter Teuben with NEMO. We acknowledge financial support for research visits in China by The Silk Road Project (2009S1-5) of Chinese Academy of Sciences, National Astronomical Observatories of China. We are thankful to Christoph Olczak for his support with the GPU nodes at the NAOC/CAS and the Titan cluster in Heidelberg, as well to Rainer Spurzem for granting access to them. This work has been supported by the Transregio 7 'Gravitational Wave Astronomy' financed by the Deutsche Forschungsgemeinschaft DFG (German Research Foundation). PA-S was supported in part by the National Science Foundation under Grant No. 1066293 and he thanks the hospitality of the Aspen Center for Physics, as well as Jorge Cuadra for his invitation to the Universidad Católica de Chile. SK was supported by the Deutsches Zentrum für Luft- und Raumfahrt and by the FONDECYT Post-doctoral Fellowship number 3130570. MC is supported by Proyecto Fondecyt Regular #1110326; BASAL Center for Astrophysics and Associated Technologies (PFB-06); FONDAP Center for Astrophysics (15010003); the Chilean Ministry for the Economy, Development, and Tourism's Programa Iniciativa Científica Milenio through grant P07-021-F, awarded to The Milky Way Millennium Nucleus; and Proyecto Anillo ACT-86. We thank Emma Robinson for comments on the manuscript. We acknowledge Antón Ricard Amaro Pendl for suggesting us to plot in B&W the clusters in the movies.

REFERENCES

Aarseth S. J., 1999, PASP, 111, 1333
Aarseth S. J., 2003, Gravitational N-Body Simulations. Cambridge Univ. Press, Cambridge
Alves-Brito A., Yong D., Meléndez J., Vásquez S., Karakas A. I., 2012, A&A, 540, A3
Amaro-Seoane P., 2006, in Merkovitz S. M., Livas J. C., eds, AIP Conf. Ser. Vol. 873, Laser Interferometer Space Antenna: 6th International LISA Symposium. Am. Inst. Phys., New York, p. 250
Amaro-Seoane P., Konstantinidis S., Miller M. C., Freitag M., Rasio F. A., 2012, ApJ, preprint (arXiv:1211.6738)
Anderson J., van der Marel R. P., 2010, ApJ, 710, 1032
Bekki K., 2011, MNRAS, 412, 2241
Bekki K., 2012, MNRAS, 421, L44
Bekki K., Yong D., 2012, MNRAS, 419, 2063
Bellini A., Piotto G., Bedin L. R., King I. R., Anderson J., Milone A. P., Momany Y., 2009, A&A, 507, 1393
Brown T. M., 2006, in Livio M., Brown T. M., eds, Space Telescope Science Institute Symp. Ser. Vol. 17, The Local Group as an Astrophysical Laboratory. Cambridge Univ. Press, Cambridge, p. 111
Brown T. M., 2009, in Jogee S., Marinova I., Hao L., Blanc G. A., eds, ASP Conf. Ser. Vol. 419, Galaxy Evolution: Emerging Insights and Future Challenges. Astron. Soc. Pac., San Francisco, p. 110
Brown T. M., Ferguson H. C., Smith E., Kimble R. A., Sweigart A. V., Renzini A., Rich R. M., VandenBerg D. A., 2003, ApJ, 592, L17
Brüns R. C., Kroupa P., 2011, ApJ, 729, 69
Brüns R. C., Kroupa P., Fellhauer M., Metz M., Assmann P., 2011, A&A, 529, A138
Buonanno R., Corsi C. E., Buzzoni A., Cacciari C., Ferraro F. R., Fusi Pecci F., 1994, A&A, 290, 69

Carretta E., Bragaglia A., Gratton R., Lucatello S., Bellazzini M., D'Orazi V., 2010a, ApJ, 712, L21
Carretta E. et al., 2010b, ApJ, 722, L1
Carretta E., Lucatello S., Gratton R. G., Bragaglia A., D'Orazi V., 2011, A&A, 533, A69
Casertano S., Hut P., 1985, ApJ, 298, 80
Catelan M., 1997, ApJ, 478, L99
Chandrasekhar S., 1969, Ellipsoidal Figures of Equilibrium. Yale Univ. Press, New Haven
Chen C. W., Chen W. P., 2010, ApJ, 721, 1790
Cohen J. G., Kirby E. N., Simon J. D., Geha M., 2010, ApJ, 725, 288
Dalcanton J. J. et al., 2009, ApJS, 183, 67
de la Fuente Marcos R., de la Fuente Marcos C., 2010, ApJ, 719, 104
de Oliveira M. R., Bica E., Dottori H., 2000, MNRAS, 311, 589
Dieball A., Grebel E. K., Theis C., 2000, A&A, 358, 144
Dieball A., Müller H., Grebel E. K., 2002, A&A, 391, 547
Fellhauer M., Kroupa P., 2002, MNRAS, 330, 642
Fellhauer M., Kroupa P., 2005, MNRAS, 359, 223
Gennaro M., Brandner W., Stolte A., Henning T., 2011, MNRAS, 412, 2469
Greissl J., Meyer M. R., Christopher M. H., Scoville N. Z., 2010, ApJ, 710, 1746
Hammer F., Yang Y. B., Wang J. L., Puech M., Flores H., Fouquet S., 2010, ApJ, 725, 542
Hurley J. R., 2003, in Makino J., Hut P., eds, Proc. IAU Symp. 208, Astrophysical Supercomputing Using Particle Simulations. Astron. Soc. Pac., San Francisco, p. 113
Hurley J. R., Pols O. R., Tout C. A., 2000, MNRAS, 315, 543
Joo S.-J., Lee Y.-W., 2013, ApJ, 762, 36
Keto E., Ho L. C., Lo K.-Y., 2005, ApJ, 635, 1062
Khalisi E., Amaro-Seoane P., Spurzem R., 2007, MNRAS, 374, 703
King I. R., 1966, AJ, 71, 64
Kroupa P., 1998, MNRAS, 300, 200
Kroupa P., 2001, MNRAS, 322, 231
Kustaanheimo P. E., Stiefel E. L., 1965, J. Reine Angewandte Math., 218, 204
Lane R. R. et al., 2010, ApJ, 711, L122
Lee J.-W., Lee J., Kang Y.-W., Lee Y.-W., Han S.-I., Joo S.-J., Rey S.-C., Yong D., 2009, ApJ, 695, L78
Makino J., Akiyama K., Sugimoto D., 1991, A&AS, 185, 63
Marino A. F. et al., 2011, A&A, 532, A8
Milone A. P., Stetson P. B., Piotto G., Bedin L. R., Anderson J., Cassisi S., Salaris M., 2009, A&A, 503, 755
Minniti D., Rejkuba M., Funes J. G., Kennicutt R. C., Jr, 2004, ApJ, 612, 215
Pancino E., Galfo A., Ferraro F. R., Bellazzini M., 2007, ApJ, 661, L155
Peacock M. B., Zepf S. E., Finzell T., 2013, ApJ, 769, 126
Perina S. et al., 2009, A&A, 494, 933
Portegies Zwart S. F., Rusli S. P., 2007, MNRAS, 374, 931
Renzini A., 2008, MNRAS, 391, 354
Riess A. G., Fliri J., Valls-Gabaud D., 2012, ApJ, 745, 156
Stephens A. W., Catelan M., Contreras R. P., 2006, AJ, 131, 1426
Stetson P. B., Catelan M., Smith H. A., 2005, PASP, 117, 1325
Theis C., 2001, in Deiters S., Fuchs B., Just A., Spurzem R., Wielen R., eds, ASP Conf. Ser. Vol. 228, Dynamics of Star Clusters and the Milky Way. Astron. Soc. Pac., San Francisco, p. 347
Valcarce A. A. R., Catelan M., 2011, A&A, 533, A120
van den Bergh S., 1996, ApJ, 471, L31
Wei L. H., Keto E., Ho L. C., 2012, ApJ, 750, 136
Whitmore B. C. et al., 2010, AJ, 140, 75

This paper has been typeset from a TEX/LATEX file prepared by the author.